A Method for Coregistration of PET and MR Brain Images

Jesper L.R. Andersson, Anders Sundin and Sven Valind

Subfemtomole Biorecognition Project, Uppsala University PET Centre, Uppsala, Sweden and Departments of Radiation Sciences, Diagnostic Radiology and Clinical Psychology, Uppsala University, Uppsala, Sweden

Combining MRI morphological data with functional PET data offers significant advantages in research as well as in many clinical situations. Automatic methods are needed, however, to coregister the data from the two modalities. **Methods:** Simulated PET images were created by simple and automatic segmentation of MR images followed by the assignment of different uptake values to various tissue types. The simulated PET images were registered to actual PET images using a pixel-by-pixel, PET-PET registration method. The transformation matrix was then applied to the MR images. The method was used to register MRI data to PET transmission scans and emission scans obtained with FDG, nomifensine and raclopride. Validation was performed by comparing the results to those obtained by matching internal points manually defined in both volumes. **Results:** Emission and transmission PET images were successfully registered to MR data. Comparison to the manual method indicated a registration accuracy on the order of 1–2 mm in each direction. No difference in accuracy between the different tracers was found. The error sensitivity for the method's assumptions seemed to be sufficiently low to allow complete automation of the method. **Conclusion:** We present a rapid, robust and fully automated method to register PET and MR brain images with sufficient accuracy for most clinical applications.

Key Words: positron emission tomography; magnetic resonance imaging; automatic image registration

J Nucl Med 1995; 36:1307–1315

The coordinated use of morphological information as assessed by MRI and functional information as assessed by PET offer great advantages and possibilities for both modalities. By complementing PET data with MRI's more reliable region of interest (ROI) definition (*1*), anatomical identification of activated areas (*2*) or local pathologies (*3*), compensation for atrophy (*4*) and better reconstruction methods (*5*) can be obtained. On the other hand, MRI can benefit from PET in the validation of new emerging methods such as functional studies with MRI (*6,7*). A prerequisite for this is accurate coregistration of the data from the two modalities to each other. A number of registration methods have been suggested to achieve this. These methods can be broadly divided into three categories: expert guided systems to match anatomical structures (*8–10*), automatic or semiautomatic systems to minimize the distance between surfaces that can be extracted in both modalities (*11–14*) and automatic methods to maximize a measure of image similarity (*15*).

Although there are specific advantages and disadvantages with each method, they seem to offer reasonably accurate registration. A disadvantage of the first category is the time an experienced worker needs to perform the registration. The second category suffers from the difficulties in automatically extracting common surfaces and from the differences in contours on images from different modalities (*13*). A disadvantage of the third category is manual editing of MR images to discard all extracerebral tissue (*15*).

In this article, we propose a method for performing PET-MRI registration that is an extension of one previously developed for PET-PET registration (*16*). By segmenting the MR images, a PET image may be simulated by assigning appropriate uptake values to cerebrospinal fluid (CSF) and to the gray and white matter. The resulting images may then be registered to the actual PET images using the PET-PET registration method. The similarity between the simulated and actual PET images will depend strongly on the accuracy of the segmentation of the MR images. The PET-PET registration method is, however, relatively insensitive to moderate differences in tracer distribution (*16*). Therefore, we believed that crude segmentation of the MRI data by simple thresholding would yield simulated PET images realistic enough to permit accurate registration. This hypothesis was tested by registering PET data obtained with several different tracers to MRI data and comparing the results to those obtained by expert-guided, point-pair matching. The method was also examined for possible sources of error.

Received Nov. 21, 1994; revision accepted Jan. 16, 1995.

For correspondence or reprints contact: Jesper Andersson, MSc, Uppsala University PET Centre, S-751 85 Uppsala, Sweden.

METHODS

PET

Scanners. Studies were performed either on a GEMS 2048-15B (*17*) or GEMS 4096-15WB (GE Medical Systems, Milwaukee, WI) (*18*) scanner. Both scanners produce 15 slices with 6.5-mm slice spacing and have 6-mm axial and transaxial FWHM.

FDG Studies. Two adults and one child (ages 39, 43 and 1 yr, respectively) underwent FDG-PET studies as part of the clinical procedure prior to surgery for complex partial epilepsy. They were positioned in the scanner so that the most basal slice corresponded to the OM line. A dose of 2.2–6.7 MBq/kg body weight of [^{18}F]FDG was injected and scanning was commenced. Data from 30 to 50 min postinjection were summed and reconstructed with a 4.2-mm Hanning filter, 2-mm pixel size, and contour finding was used for attenuation correction (*19*). Due to the risk of seizures, the only fixation was foam padding supported by a plexiglass head rest. The child was sedated throughout the examination to prevent excessive movements.

Carbon-11-Nomifensine and Carbon-11-Raclopride Studies. Carbon-11-nomifensine and ^{11}C-raclopride studies were performed in four individuals (ages 53, 54, 55 and 60 yr) randomly selected from a group of 15 volunteers participating in a project studying the effects of organic solvents. The volunteers had been exposed to organic solvents in their line of work (painters) but had apparently normal MRI scans. They were positioned in the scanner so that the most basal slice corresponded to the OM line. Fixation was achieved through foam padding supported by a plexiglass head rest and a broad adhesive tape across the forehead attached to the head rest. A dose of 3.8–8.3 MBq/kg body weight ^{11}C-nomifensine and 1.7–4.0 MBq/kg body weight ^{11}C-raclopride was injected. Data from 7 to 29 min postinjection were summed for both tracers and images were reconstructed with a 4.2-mm Hanning filter and 2-mm pixel size. All raclopride scans and two of the nomifensine scans were reconstructed using a transmission scan for attenuation correction; the other two nomifensine scans used contour finding (*19*). The study from which data were taken was approved by the Ethics Committee of the Medical Faculty, University of Uppsala and by the Isotope Committee, Uppsala University Hospital. Informed consent was obtained from all subjects.

MRI

Scanning was performed with a spin-echo pulse sequence with echo times ranging from 20 to 25 msec and repetition times between 520 and 550 msec in six subjects. For a seventh subject, a turbo spin-echo sequence with 12-msec echo time and 540-msec repetition time was used. Images were sampled as transaxial 6 mm thick 256 × 256 matrices with pixel sizes between 0.78 and 0.90 mm and a slice gap of 0.6 mm. The number of slices varied between 19 and 23 but covered the entire cerebrum in all cases. Fixation was achieved in a manner similar to that for PET scanning. Images were converted from their internal format to ACR-NEMA files for export to the PET computer system where they were converted to the vendor-specific file format used for PET images. In the last conversion step, adjacent pixels were averaged to create 128 × 128 matrices with twice the original pixel size.

PET-MRI Registration

Computers. A VAX-station 4000/60 (Digital Equipment Corp., Maynard, MA) was used for all calculations. The programs performing calculations were written in C and were linked to libraries written in FORTRAN delivered with the scanner and to routines copied from Press et al. (*20*).

TABLE 1
Uptake Values for Different Types of Tissue Used When Creating Simulated PET Images

	Tissue type				
Tracer	Air	Ventricle and bone	White matter	Gray matter	Subcutaneous fat
FDG	0	0	1	4	0
^{11}C-nomifensine	0	0	1	4	0
^{11}C-raclopride	0	0	1	2	2
Transmission	0	1	1	1	1

Coordinate Axes. The coordinate system was defined so that the x-axis runs transaxially in the left-right direction, the y-axis runs transaxially in the up-down direction and the z-axis runs axially. The letter α is used to denote rotation around the x-axis, β rotation around the y-axis and γ rotation around the z-axis. The origins of the systems are defined as the geometrical center point of the two image volumes, respectively.

Creation of Simulated PET Images. The voxels of the MR images were classified as consisting of either air, ventricle and bone, white matter, gray matter or subcutaneous fat. Classification was performed by simple thresholding. To simulate a PET scan, each tissue category was given an uptake value that was dependent on tracer type. All uptake values used in this study are presented in Table 1. The simulated PET scan was then filtered with a two-dimensional Gaussian filter to yield an inplane FWHM of approximately 7.0 mm, which is comparable to that in the actual PET images.

To obtain full automation of the method, the thresholds for each study had to be obtained automatically, or the same thresholds would have to be used for all individuals. To do the latter would not be practical since the interindividual variation is large and a separate set of thresholds would have to be evaluated for each MRI protocol. An attempt to fit a number of Gaussians equal to the number of tissue types for data segmentation to histographic representation of all voxels in the volume did not yield satisfactory results due to insufficient separation between gray and white matter and was therefore ruled out. We assumed instead that the relative abundance of the four types of tissue, as measured by MRI, was roughly equal across subjects. Given that assumption and the fact that 35% of all nonair voxels in a T1-weighted MRI volume consist primarily of bone and ventricle, an upper threshold for bone and ventricle (and thus also a lower threshold for gray matter) could be estimated by integrating histographic representation of all nonair voxels until the integral spans 35% of the voxels. To obtain the upper threshold for gray matter, the histogram was integrated from the upper threshold for bone and ventricle until the integral spans the relative abundance of gray matter, etc.

To obtain standard values for the relative abundance of the different tissue types, the following strategy was applied. The remaining 11 volunteers had MRI scanning according to the protocol above. Data were transferred to the PET system and analyzed with the vendor-supplied image display system. By inserting monochromatic bands into the color scale and interactively moving these over the scale, approximate thresholds between the different types of tissue were subjectively assessed. These thresholds, together with the appurtenant MRI volume, were fed to a voxel-count program that counted all nonair voxels in the volume that fell in each tissue category. Thus, estimates of the relative abundance of each tissue category were obtained for each of the 11 subjects. Since this value is clearly dependent on the exact area of the brain spanned during the examination, only data from the first slice in which the temporal lobes were visible to the last slice containing cerebral tissue of the vertex were used by the voxel count program.

These standard values were then used to estimate thresholds for the seven subjects in the validation study by creating histograms of all nonair voxels from all slices above the temporal poles and integrating them. The thresholds were then applied to all slices in the MRI volume and to those below the temporal poles.

Registration. Registration of the simulated images to the actual PET images was achieved using a previously described pixel-by-pixel image similarity method (*16*) that operates on pixels with a high signal-to-noise ratio only. These pixels were identified by differentiating the reference image volume (the fixed volume) and creating a mask by thresholding the derivative volume so that only 10% of pixels with the highest data content in the volume are used. This was a small modification from the PET-to-PET registration procedure in which only 5% of the pixels were used. By performing the differentiation on the simulated PET images, the effects from high localized uptakes (e.g., ^{11}C-raclopride in the caudate nucleus) were minimized since these structures were not covered by the mask. In PET-to-PET registration, the method behaves robustly and no local maxima seem to exist in a reasonable vicinity of the true solution (*16*).

Our experience of registering MRI to PET images indicates that local maxima are a problem in this context, possibly due to initial misregistrations being larger, or to the superficial similarity between the simulated and measured PET images. To overcome this problem, multiple starting points were used. Six initial preregistrations with an extensive subsampling of the volume and liberal convergence criteria were performed. The starting values for axial translation head tilting in the anterior-posterior direction were varied between the registrations. These parameters were varied because they were frequently found to differ substantially between the PET and MRI volumes. The results from the initial preregistrations were checked, and the values resulting in the largest maxima were chosen as starting values for the final registration.

Validation

Equivalent Internal Points (EIP). An expert-guided landmark registration method was used as an independent method to validate automatic registration. PET and MRI datasets were resampled to yield twenty-nine 128 × 128 × 2.0-mm slices with a 4.5-mm slice thickness. PET and MRI images were shown concurrently in a modified version of the image display and manipulation software provided by the manufacturer, and homologous point-pairs in the two image sets were identified and their positions recorded. The software allows reslicing of the image volumes in any direction to aid in the identification of landmarks. The landmarks were selected independently by three individuals experienced in studying tomographic images and consisted of structures identifiable in both modalities such as the caudate nucleus head, the thalamus and points on the cortical surface with high curvature. The exact location and number of points varied depending on the characteristics of the PET tracer used. For tracers providing little anatomical information (e.g., raclopride), a combination of points identified in the emission and transmission images was used. The transformation matrix mapping the PET dataset onto the MRI dataset was obtained by minimizing the sum of the Euclidean distances between the paired points with nonlinear fitting.

TABLE 2
Relative Abundance of Different Types of Tissue in the Standard Group

Tissue type	Relative tissue abundance (%) Mean	s.d.	Range
Ventricle and bone	38.4	3.4	33.6 – 46.8
Gray matter	27.7	2.2	25.3 – 33.6
White matter	24.0	3.6	19.4 – 32.0
Subcutaneous fat	9.9	3.9	4.9 – 16.4

Emission-Transmission Comparison. Emission scans and transmission scans were obtained during the same scanning session. It was assumed that there had been no subject movement between the scan sessions and both the emission and transmission data were registered to the MRI data. A comparison of the emission data to the transmission data enabled estimation of registration process errors, if there were no systematic errors also affecting the method when emission and transmission data are used.

Error Analysis

Registration with and without Editing Extracerebral Structures. To determine the method's sensitivity to the presence of extracerebral tissue in MR images, the registration was carried out both with and without manual editing of the MRI data to discard extracerebral tissue such as the scalp, meningies and large vessels. Data were edited with vendor-supplied image display and analysis software and consisted of manually defining ROIs around the brain and setting all voxels outside the ROIs to zero. This was done for all seven MRI examinations used in the validation study. When the edited MR images were segmented, the same threshold values for the nonedited data were used.

Registration with Different Standard Values for Tissue Composition. If the method is to be completely automatic in its present form, the same standard values for relative tissue abundance must be used for all, or close to all, individuals. Table 2 shows the spread of these values encountered in 11 subjects on the order of 3%–4% for each type of tissue with a range of 10%–15%. To examine the effect on individuals with a tissue composition significantly different from that in our standard group, registration was performed with different combinations of tissue composition values. The values for relative abundance of subcutaneous fat and CSF were varied, and the values for the other types of tissue were adjusted accordingly to ensure a total of 100%. We varied the values for fat and CSF because they were expected to be the more differing parameters (e.g., in obese individuals or in individuals with marked cerebral atrophy).

RESULTS

Standard Values for Relative Tissue Abundance.

Values for relative tissue abundance obtained from the standard group are presented in Table 2. These values are in no way intended as a statement on actual tissue composition, but rather, represent values for practical use for this registration method only. The ranges for relative abundance of CSF and bone and subcutaneous fat are on the

FIGURE 1. Outputs from the various steps in the registration process. (A) T1-weighted MR image. (B) Simulated PET image created from the MR image in A, using uptake values for ^{11}C-nomifensine from Table 1. (C) Mask consisting of 10% of the voxels of the simulated PET volume (shown in B) with the highest derivative values. Note how a mixture of brain surface regions and borders between gray and white matter are used in the registration. (D) Carbon-11-nomifensine PET image after registration. (E) The same MR image as in A. (F) Simulated PET image created from the MR image in E, using uptake values for ^{11}C-raclopride from Table 1. (G) Mask consisting of the 10% of the voxels of the simulated PET volume (shown in F) with the highest derivative values. (H) Carbon-11-raclopride PET image after registration. The image is scaled so that the maximum of the gray scale is at 40% of the maximum intensity in the basal ganglia.

order of 15% and 10%, respectively. Thus, the range for values to assess error sensitivity these assumptions was larger than that encountered in this material.

Automatic Registration

All examinations used for the validation were successfully registered with the automatic method and the results looked qualitatively good. No apparent misregistrations could be identified by visual inspection of the images. Local maxima presented no problems with the multiple starting point approach. The average CPU time for the entire registration process, exclusive of I/O and file transfer, was 190 sec (range 168–221 sec). Two examples of simulated PET images and the resulting masks are shown in Figure 1. The different uptake values for various tracers result in using different parts of the images for the registration. Figure 2 shows registered FDG, nomifensine and raclopride PET images overlaid on MR images. There was good qualitative agreement between the images.

Equivalent Internal Point Registration

The mean number of point pairs and the mean error per point pair are shown for each tracer in Table 3. The interobserver variability is shown in Table 4. Table 4 indicates a somewhat larger spread of the translation in the axial direction and the rotation around the x-axis compared to the other directions. This is in agreement with a general opinion, shared by all observers, that accurate identification was hardest to achieve in the axial direction. The larger spread for raclopride than for the other tracers is also in accordance with the difficulties experienced by all observers in identifying points in the raclopride emission images and in the transmission images. The performance of the EIP method depends on the experience and skill of the observers and the versatility of the software used. Therefore, the values for interobserver spread reflect the performance of the method in our facility and cannot be extrapolated to other sites without reservations.

Automatic Versus EIP Registration

The differences between the results of the present method and the EIP method are presented in Table 5 and in Figure 3. A comparison of Tables 4 and 5 indicates that the difference was of approximately the same magnitude as the interobserver spread of the EIP method. For the raclo-

FIGURE 2. Registered PET images overlaid on T1-weighted MR images. Images were created by mapping the MR images into a gray scale and the PET images into the Sokoloff pseudocolor scale. Every other screen pixel was given a hue of gray from the MR image, and every other was given a color from the PET image. (A) FDG image registered to MR image. (B) Nomifensine image registered to MR image. (C) Raclopride image registered to MR image from the same individual as in B.

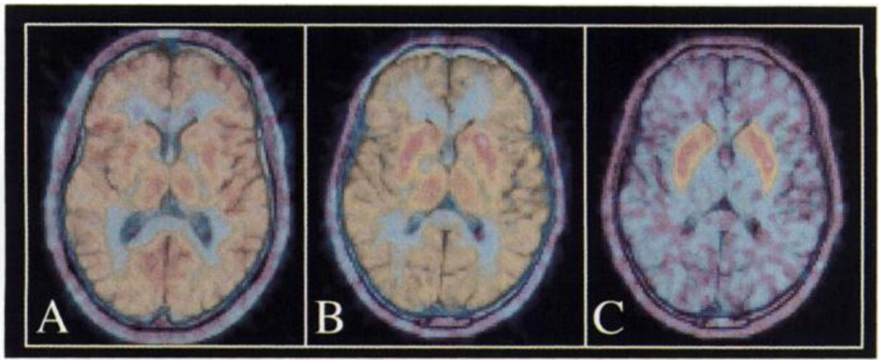

TABLE 3
Statistics Regarding Registration with the EIP Method

Tracer	No. of points	Mean error per point* (mm)
FDG	12.8 ± 1.6	4.05 ± 1.27
Nomifensine	13.4 ± 1.7	4.10 ± 1.03
Raclopride	10.8 ± 1.4	4.58 ± 1.67

*The mean remaining Euclidean distance between the corresponding points in the two volumes after the transformation of one of the volumes according to the transformation matrix that minimized this measure.

pride studies, the difference between the two methods was surprisingly small given the large interobserver variability for the EIP method. This may well be an effect of the small numbers.

Registration of Emission Versus Transmission PET Images

The results from coregistered MR and PET emission images compared to PET transmission images are shown in Table 6 and Figure 4. The magnitude of the differences was of the same order as the differences between the EIP method and automatic registration to the emission images (Table 5). There is the possibility of subject movement between the emission and the transmission scan, which adds to the estimated uncertainty of the method.

Registration with and without Editing of Extracerebral Structures

The errors resulting from registration of PET data to MR images from which extracerebral tissue had been edited are shown in Table 7. Strangely, there seems to be a tendency towards larger errors when edited (Table 5) MRI data are used. The effect, however, does not reach conventional significance. An explanation for this may be offered by Figure 1, where the existence of the scalp in the MR images clearly yields a higher degree of similarity between the actual and simulated PET images, especially for raclopride (Figs. 1F, H) and for nomifensine (Figs. 1B, D), than if it had not been present.

Registration with Different Standard Values for Tissue Composition

Results from the registrations performed with different assumptions for relative tissue abundance are shown in Table 8 and Figure 5. The analysis indicates that this is not a sensitive parameter and no significant difference beween the errors (paired t-test) for any two assumptions for relative abundance of subcutaneous fat or bone and CSF was found. The lack of significance, however, should not be overemphasized given the small numbers.

TABLE 4
Interobserver Spread for Registration with the EIP Method

		Translation (mm)			Rotation (deg)		
Tracer	n	X	Y	Z	α	β	γ
FDG	3	0.69* ± 0.22†	0.83 ± 0.23	1.95 ± 1.27	1.23 ± 0.29	0.84 ± 0.17	0.78 ± 0.24
Nomifensine	4	0.73 ± 0.13	0.48 ± 0.47	1.80 ± 1.30	1.37 ± 0.65	0.61 ± 0.35	0.70 ± 0.27
Raclopride	4	0.79 ± 0.50	0.97 ± 0.40	4.38 ± 2.69	3.22 ± 1.39	1.18 ± 0.80	0.76 ± 0.78

*The mean value of the interobserver spread (the standard deviation over the observers) averaged over all subjects analyzed with that tracer.
†The standard deviation of interobserver spread when averaged over all subjects analyzed with that tracer.

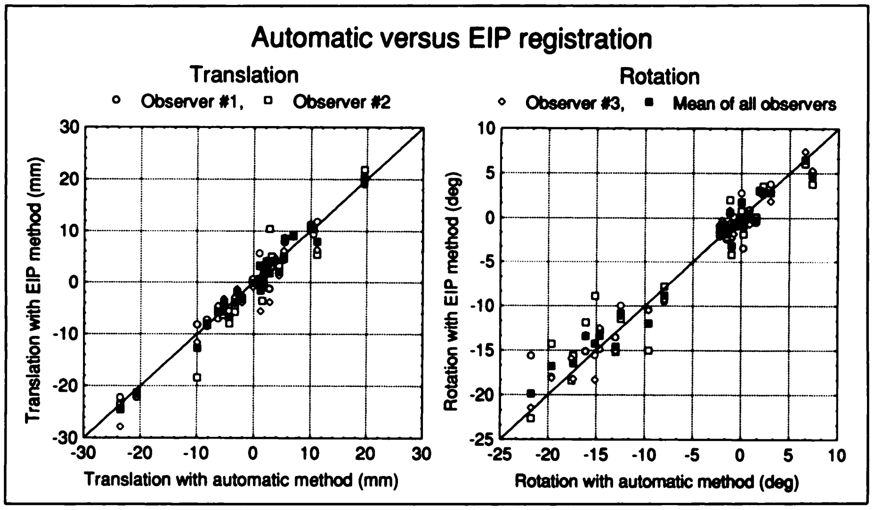

FIGURE 3. A comparsion between the results obtained from the automatic method and the EIP method. Translation is shown on the left and rotation on the right. Translation along all axes and rotation around all axes are lumped. The scaling of the axes are different for the two graphs.

TABLE 5
Registration Error in All Directions for the Examined Tracers

		Translation (mm)			Rotation (deg)		
Tracer	n	X	Y	Z	α	β	γ
FDG	3	0.53[*] ± 0.33[†]	1.41 ± 1.00	1.37 ± 0.57	1.25 ± 0.37	1.29 ± 0.92	1.66 ± 1.01
Nomifensine	4	0.33 ± 0.27	1.08 ± 0.61	1.79 ± 1.11	1.58 ± 0.90	0.67 ± 0.51	0.46 ± 0.14
Raclopride	4	1.44 ± 0.74	0.93 ± 1.26	1.96 ± 1.34	1.94 ± 0.79	1.17 ± 0.74	1.10 ± 0.74

---

[*] The mean value of the absolute values of the difference between the result obtained with the automatic method and the result obtained with the EIP method averaged over the three observers.

[†] The standard deviation of the absolute values of the difference between the automatic method and the EIP method averaged over the three observers.

DISCUSSION

The validation of an intermodality registration method is a complex problem that has been discussed by Neelin et al. (*21*) and can be described as follows: When using actual data from scans obtained on humans, the true answer cannot be known and any validation involves comparing the validation method to an independent method which will also have errors. Thus, the registration errors measured in that way will always be overestimated, and the results may be limited by the reference method rather than the method being tested. On the other hand, when phantom measurements combined with fiducial markers (*22*) or simulated data (*21*) are used, the true answer is known but the question is how representative is the validation for real human data. When validating the method presented in this article, the use of simulated data would clearly yield a situation with circular evidence and was therefore not applicable. The use of phantoms may yield data suitable for validation of surface-fit methods, in which the important criterion is to obtain realistic head or cortical surfaces. In our method, however, it would not suffice. First, segmentation of the MRI data would be trivial, which is certainly not the case for human data. Second, extracerebral tissue effects that could potentially cause problems for a method of this kind could not be mimicked by a phantom.

Thus, we decided to use actual data and compared the results with those from the EIP method (*8,23,21*). In a recent paper (*24*), the EIP method was found to be superior to a number of other registration methods, including the surface-fit method and the stereotactic z-frame.

Our results, with mean errors in the order of 1.5 mm in each direction, are slightly worse than those obtained by Woods et al. (*15*) using a similar method. There could be many reasons for this. First, the validation method used by Woods et al. (*15*) is most probably superior to the EIP method. They used what is essentially the z-frame method but the z-shaped fiducial is attached to the subject's skull rather than to a head holder in which the subject is more or less fixed. Their measurements of fiducial-based registration errors, supported by measurements by Ge et al. (*25*) on a similar system, indicate submillimeter accuracy. This should be compared to mean errors for the EIP method on the order of a 1.3-mm translation in each direction and 1.7° around each axis (*21*) and to the interobserver spread for the EIP method encountered in this article (Table 4). The errors presented in Table 5 represent a combination of the errors in our method and in the validation method, in which the relative contributions of each method are unknown.

Second, the slice thickness of the MRI data in this study is relatively large and yields highly anisotropic voxels. Due to the nonlinearity of the PET image simulation process, the partial volume effects resulting from large slice thickness will affect PET and MRI data differently. This occurs because the order of the intensity of the various tissue types is different in T1-weighted MR images CSF) compared to PET images for most tracers (gray>white>CSF).

TABLE 6
Comparison between Registration of MR Images to PET Transmission and Emission Images

		Translation (mm)			Rotation (deg)		
Tracer	n	X	Y	Z	α	β	γ
Nomifensine	2	0.42[*] ± 0.43[†]	0.41 ± 0.41	1.37 ± 1.30	2.04 ± 0.50	1.20 ± 1.17	0.50 ± 0.09
Raclopride	4	0.51 ± 0.18	0.86 ± 0.24	1.95 ± 0.65	1.50 ± 0.57	1.30 ± 1.14	0.68 ± 0.53

---

[*] The mean value of the absolute values of the difference between coregistered MR and PET emission images and transmission images averaged over all subjects analyzed with that tracer.

[†] The standard deviation of the absolute values of the difference between coregistered MR and PET emission and transmission images when averaged over all subjects analyzed with that tracer.

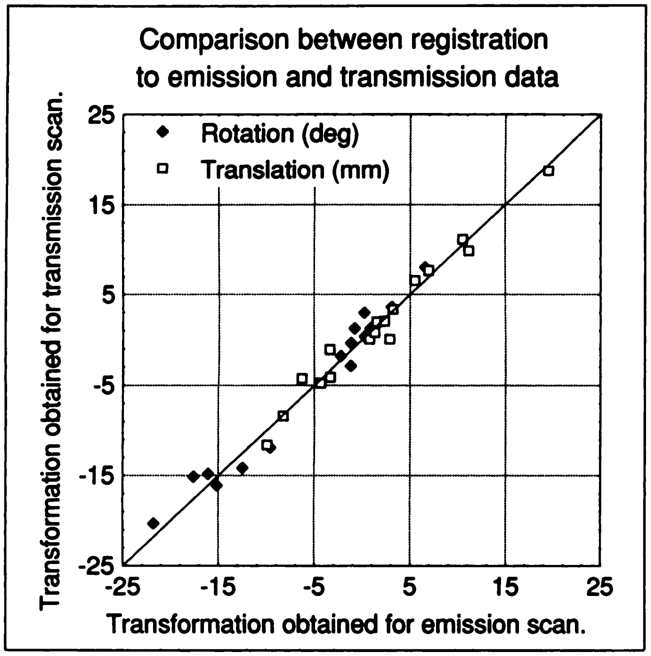

FIGURE 4. Comparison of coregistered MR images to PET emission and transmission images. Translation along all axes and rotation around all axes are lumped.

Hence, when segmenting MR images, there will be a rim on the cortex surface that is classified as CSF. The width of this rim will increase with increasing angles of the surface through the imaging plane. Similarly, on the borders between white matter and CSF, there will be a rim classified as gray matter. The effect will again be accentuated with increasing angles of the border through the image plane. Thus, there will be a combined effect of apparent movement of cortical surface and of false rims of high activity around the ventricles which varies throughout the volume. Thinner slices and/or possibly other MRI sequences yielding intensities in the MR images in the same order as for most PET tracers (e.g., proton density-weighted images) would alleviate this and probably result in higher registration accuracy. The accuracy will be sufficient for most clinical and scientific studies, and it may be advantageous to validate the method on MRI studies with thick slices and highly anisotropic voxels since these types of studies are used in most clinical examinations of the brain.

The method presented in this article has many similarities to the one suggested by Woods et al. (*15*) but differs from it in two important aspects. First, our methodology involves explicit, albeit primitive, segmenting of MR images using information about tissue composition and the creating simulated PET images with data of relative uptake in different tissue types for the specific tracer. In the algorithm suggested by Woods et al. (*15*), the segmentation and assignment of uptake values is performed implicitly by grouping the MRI pixels into 256 groups for which separate means and standard deviations are evaluated. Although elegant and self-adapting, their strategy implies that the iterative process, apart from evaluating the transformation matrix, is also responsible for creating simulated PET images from the MRI images. Thus, the problem will be worsened, which implies longer execution times, more local maxima and a less certified convergence. This effect is demonstrated by the considerably longer execution times reported for PET-MRI registration (*15*) than for PET-PET registration (*26*) and by the lack of convergence when extracerebral tissue is present in the MR images (*15*). With the explicit segmentation and simulation of additional information in our method, the problem gets better conditioning, yields faster and more reliable convergence and allows the existence of scalp and meningies in MR images. The disadvantages are the need to explicitly specify uptake patterns for every tracer used and the risk of introducing systematic errors. The latter seem not to be the case given that our validation results do not indicate any bias. The second difference lies in the use of a mask based on the derivatives in the volume of simulated PET images. As seen in Figure 1G, this results in automatic exclusion of the basal ganglia from the registration process, which allows raclopride PET scans to be aligned with MRI scans.

The present method can also register PET transmission images to MRI data. This is an important feature since some tracers (e.g., CO) exhibit uptake patterns that will not allow direct registration to emission images with any method. Registration of MRI data to the emission data is always advantageous since possible errors from movement between the transmission and emission scanning sessions is avoided.

The 3-min execution speed compares favorably to those

TABLE 7
Registration Error in All Directions for the Study Tracers with Extracerebral Tissue Removed from the MR Images

		Translation (mm)			Rotation (deg)		
Tracer	n	X	Y	Z	α	β	γ
FDG	3	0.64[*] ± 0.06[†]	3.00 ± 1.66	1.32 ± 0.41	1.53 ± 1.16	2.00 ± 1.50	1.01 ± 1.15
Nomifensine	4	0.43 ± 0.30	0.54 ± 0.51	1.64 ± 1.14	1.81 ± 0.91	0.62 ± 0.56	0.54 ± 0.19
Raclopride	4	1.41 ± 0.63	1.47 ± 1.06	2.24 ± 1.62	3.17 ± 2.22	1.24 ± 0.33	1.49 ± 0.74

---

[*] The mean value of the absolute values of the difference between the automatic and EIP methods averaged over the three observers.

[†] The standard deviation of the absolute values of the difference between the automatic method and EIP methods averaged over the three observers.

TABLE 8
Registration with Different Tissue Compositions

Tissue composition	Nomifensine		Raclopride	
	Translation (mm)	Rotation (deg)	Translation (mm)	Rotation (deg)
Standard	1.07* ± 0.92†	0.90 ± 0.74	1.44 ± 1.13	1.40 ± 0.79
5% Fat	1.11 ± 1.05	0.85 ± 0.61	1.44 ± 1.23	1.45 ± 0.73
15% Fat	1.14 ± 0.96	0.90 ± 0.80	1.65 ± 1.07	1.70 ± 1.19
20% Fat	1.14 ± 0.71	0.92 ± 0.88	1.65 ± 1.12	1.66 ± 1.05
30% Ventricle	1.11 ± 0.76	1.00 ± 1.04	1.56 ± 1.07	1.41 ± 0.92
35% Ventricle	1.09 ± 0.87	0.88 ± 0.81	1.53 ± 1.04	1.73 ± 1.13
45% Ventricle	1.18 ± 1.15	0.82 ± 0.61	1.48 ± 1.28	1.56 ± 0.88
50% Ventricle	1.39 ± 1.50	0.74 ± 0.50	1.76 ± 1.62	1.56 ± 1.29

---

*The mean value of the absolute values of the difference between the automatic and EIP methods averaged over all subjects and all three directions.

†The standard deviation of the absolute values of the difference between the automatic and EIP methods when averaged over all subjects and all three directions.

reported by other groups and is obtained by excluding most of the data from the registration process with a derivative mask. A high execution speed, however, is less an issue for MRI-PET registration since considerably fewer registrations are done. When PET images are coregistered, there are typically six or more studies to register, as in activation studies, or multiple frames to register to the first frame, as in dynamic protocols. Also, the other steps involved in transferring MRI data to the PET system, or vice versa, are so time-consuming that the time spent on registration is only a small part of the total process.

An important property of our method is that it is completely automatic. Previous attempts in this direction have often involved manual interaction at some part in the process such as manual definition or editing brain contours (*11,13*) or editing MRI data to discard extracerebral voxels (*15*). If the method is to be completely automatic, the values for relative tissue abundance from the standard group must be applicable to the large majority examinations to be registered. The fact that the values were collected from one group and applied to another heterogeneous group supports this notion. For subjects with extensive atrophy, individual limits will have to be estimated with the same technique used for the standard group. This process is not time-consuming and typically takes a few minutes.

The presence of large pathologies (e.g., tumors or ischemic areas) in the images may present difficulties. Such areas also affect the results of PET-PET registrations (*16*). For PET-PET images, errors may be avoided by manually defining the area, drawing an ROI around it and discarding it from the registration process (*16*). The same strategy can probably be applied to PET-MRI images.

The present method has also successfully registered T2-weighted MR images to PET images (data not shown). Modifications to the method were limited to the collection of new "standard values," since CSF and bone cannot be lumped together for T2-weighted data. It is expected that the application of the present method to any type of MRI sequence (with reasonable separation between the principle types of tissue) should be equally smooth.

CONCLUSION

Registration of MR and PET images is an important step toward realizing the full potential of both imaging modali-

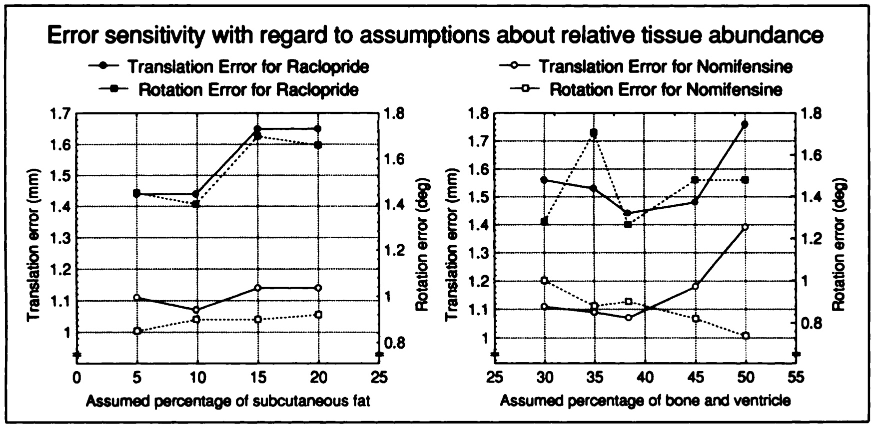

FIGURE 5. The left panel shows registration error changes when assumptions about relative abundance of subcutaneous fat vary. The right panel shows the error changes when the assumptions about relative abundance of bone and ventricle vary. Registration errors are lumped along all directions and around all axes.

ties. Our methodology can automatically register MR images to PET images obtained with a wide variety of tracers and with an accuracy of 1–2 mm in each direction.

ACKNOWLEDGMENTS

The authors thank Harald Schneider for technical support; Karin Lidström for manual editing of MRI data; Britt-Marie Bolinder for assistance with the retrieval of MRI data; and Björn Hellman, Christer Edling and The Swedish Work Environment Fund (project 91-02-13) for providing some of the material used in this study.

REFERENCES

1. Evans AC, Marret S, Torrescorzo J, Ku S, Collins L. MRI-PET correlation in three dimensions using a volume-of-interest (VOI) atlas. *J Cereb Blood Flow Metab* 1991;11:A69–A78.
2. Ishii K, Senda M, Bando M, et al. Application of single subject $H_2{}^{15}O$ activation study with PET-MRI registration to the patophysiological analysis in primary progressive aphasia. In: Uemura K, Lassen NA, Jones T, Kanno I, eds. *Quantification of brain function, tracer kinetics and image analysis in brain PET*. Amsterdam: Elsevier; 1993:597–603.
3. Scott AM, Macapinlac H, Zhang JJ, et al. Clinical applications of fusion imaging in oncology. *Nucl Med Biol* 1994;21:775–784.
4. Müller-Gärtner HW, Links JM, Prince JL, et al. Measurement of radiotracer concentration in brain gray matter using positron emission tomography: MRI-based correction for partial volume effects. *J Cereb Blood Flow Metab* 1992;12:571–583.
5. Ardekani BA, Braun M, Hutton BF. Improved quantification with the use of anatomical information in PET image reconstruction. In: Uemura K, Lassen NA, Jones T, Kanno I, eds. *Quantification of brain function, tracer kinetics and image analysis in brain PET*. International congress series no. 1030; 1993:351–359.
6. Belliveau JW, Kennedy DN, McKinstry RC, et al. Functional mapping of the human visual cortex by magnetic resonance imaging. *Science* 1991;254: 716–719.
7. Cohen MS, Bookheimer SY. Localization of brain function using magnetic resonance imaging. *Trends Neurosci* 1994;17:268–277.
8. Evans AC, Marret S, Collins L, Peters TM. Anatomical-functional correlative analysis of the human brain using three-dimensional imaging systems. *SPIE Medical Imaging III: Image Processing* 1989;1092:264–274.
9. Pietrzyk U, Herholz K, Heiss WD. Three-dimensional alignment of functional and morphological tomograms. *J Comput Assist Tomogr* 1990;14:51–59.
10. Greitz T, Bohm C, Holte S, Eriksson L. A computerized brain atlas: construction, anatomical content and some applications. *J Comput Assist Tomogr* 1991;15:26–38.
11. Pelizzari C, Chen G, Spelbring D, Weichselbaum R, Chen CT. Accurate three-dimensional registration of CT, PET and/or MRI images of the brain. *J Comput Assist Tomogr* 1989;13:20–26.
12. Steinmetz H, Huang Y, Seitz RJ, et al. Individual integration of positron emission tomography and high resolution magnetic resonance imaging. *J Cereb Blood Flow Metab* 1992;12:919–926.
13. Jiang H, Robb RA, Holton KS. A new approach to three-dimensional registration of multimodality medical images by surface matching. *SPIE Visualization in Biomedical Computing* 1992;1808:196–213.
14. Mangin JF, Frouin V, Bloch I, Bendriem B, Lopez-Krahe J. Fast nonsupervised three-dimensional registration of PET and MR images of the brain. *J Cereb Blood Flow Metab* 1994;14:749–762.
15. Woods RP, Mazziotta JC, Cherry SR. MRI-PET registration with automated algorithm. *J Comput Assist Tomogr* 1993;17:536–546.
16. Andersson JLR. A rapid and accurate method to realign PET scans utilizing image edge information. *J Nucl Med* 1995;36:657–669.
17. Holte S, Eriksson L, Dahlbom M. A preliminary evaluation of the Scanditronix PC2048-15B brain scanner. *Eur J Nucl Med* 1989;15:719–721.
18. Kops R, Herzog H, Schmid A, Holte S, Feinendegen L. Performance characteristics of an eight-ring, whole-body PET scanner. *J Comput Assist Tomogr* 1990;14:437–445.
19. Bergström M, Litton J, Eriksson L, Bohm C, Blomqvist G. Determination of object contour from projections for attenuation correction in cranial positron emission tomography. *J Comput Assist Tomogr* 1982;6:365–372.
20. Press WH, Flannery BP, Teukolsky SA, Wetterling WT. *Numerical recipies in C. The art of scientific computing*. New York: Cambridge University Press; 1988:291–317.
21. Neelin P, Crossman J, Hawkes DJ, Ma Y, Evans AC. Validation of an MRI/PET landmark registration method using three-dimensional simulated PET images and point simulations. *Comput Med Imag Graph* 1993;17:351–356.
22. Turkington TG, Jaszczak RJ, Pelizzari CA, et al. Accuracy of registration of PET, SPECT and MR images of a brain phantom. *J Nucl Med* 1993;34: 1587–1594.
23. Pelizzari CA, Evans AC, Neelin P, Chen C-T, Marret S. Comparison of two methods for three-dimensional registration of PET and MRI images. *Proc IEEE-EMBS* 1991;13:221–223.
24. Anderson JR, Strother SC, Xu X-L, Bonar DC, Rottenberg DA. Error bounds for five image registration techniques based on high resolution MRI. In: Uemura K, Lassen NA, Jones T, Kanno I, eds. *Quantification of brain function, tracer kinetics and image analysis in brain PET*. Amsterdam: Elsevier; 1030; 1993:429–435.
25. Ge Y, Fitzpatrick JM, Votaw JR. Retrospective registration of PET and MR brain images: an algorithm and its stereotactic validation. *J Comput Assist Tomogr* 1994;18:800–810.
26. Woods RP, Cherry SR, Mazziotta JC. Rapid automated algorithm for aligning and reslicing PET images. *J Comput Assist Tomogr* 1992;16:620–633.